# An atomic hydrogen bridge fueling NGC 4418 with gas from VV 655

E. Varenius<sup>1</sup>, F. Costagliola<sup>1</sup>, H.-R. Klöckner<sup>2</sup>, S. Aalto<sup>1</sup>, H. Spoon<sup>3</sup>, I. Martí-Vidal<sup>1</sup>, and J. E. Conway<sup>1</sup>

- Department of Space, Earth and Environment, Chalmers University of Technology, Onsala Space Observatory, 439 92 Onsala, Sweden. e-mail: varenius@chalmers.se
- Max-Planck-Institut f
  ür Radioastronomie, Auf dem H
  ügel 69, 53121 Bonn, Germany
- Ornell Center for Astrophysics and Planetary Science, Space Sciences Building, Ithaca, NY 14853, USA

Submitted to Astronomy & Astrophysics

#### **ABSTRACT**

Context. The galaxy NGC 4418 harbours a compact ( $< 20\,\mathrm{pc}$ ) core with a very high bolometric luminosity ( $\sim 10^{11}\mathrm{L}_\odot$ ). As most of the galaxy's energy output comes from this small region, it is of interest to determine what fuels this intense activity. An interaction with the nearby blue irregular galaxy VV 655 has been proposed, where gas aquired by NGC 4418 could trigger intense star formation and/or black hole accretion in the centre.

Aims. We aim to constrain the interaction hypothesis by studying neutral hydrogen structures which could reveal tails and debris connecting NGC 4418 to the nearby galaxy VV 655.

Methods. We present observations at 1.4 GHz with the Very Large Array (VLA) of radio continuum as well as emission and absorption from atomic hydrogen. Gaussian distributions are fitted to observed HI emission and absorption spectra. We estimate the star formation rate (SFR) of NGC 4418 and VV 655 from the 1.4 GHz radio emission and compare with estimates from archival  $70\,\mu m$  Herschel observations.

Results. An atomic HI bridge is seen in emission, connecting NGC 4418 to the nearby galaxy VV 655. While NGC 4418 is bright in continuum emission and seen in HI absorption, VV 655 is barely detected in the continuum but show bright HI emission ( $M_{\rm HI} \sim 10^9 \, \rm M_{\odot}$ ). We estimate SFRs from the 1.4 GHz continuum of 3.2  $\rm M_{\odot} \, yr^{-1}$  and 0.13  $\rm M_{\odot} \, yr^{-1}$  for NGC 4418 and VV 655 respectively. Systemic HI velocities of  $2202 \pm 20 \, \rm km \, s^{-1}$  (emission) and  $2105.4 \pm 10 \, \rm km \, s^{-1}$  (absorption) are measured for VV 655 and NGC 4418 respectively. Redshifted HI absorption is seen ( $v_c = 2194.0 \pm 4.4 \, \rm km \, s^{-1}$ ) towards NGC 4418, suggesting gas infall. North-west of NGC 4418 we detect HI in emission, blueshifted ( $v_c = 2061.9 \pm 5.1 \, \rm km \, s^{-1}$ ) with respect to NGC 4418, consistent with an outflow perpendicular to the galaxy disk. We measure a deprojected outflow speed of 178 km s<sup>-1</sup> which, assuming simple cylindrical model, gives an order of magnitude estimate of the HI mass outflow rate of  $2.5 \, \rm M_{\odot} \, yr^{-1}$ .

Conclusions. The morphology and velocity structure seen in HI is consistent with an interaction scenario, where gas was transferred from VV 655 to NGC 4418. Some gas is falling towards NGC 4418, and may fuel the activity in the centre. We interpret blueshifted HI-emission north-west of NGC 4418 as a continuation of the outflow previously discussed by Sakamoto et al. (2013), powered by star formation and/or black hole accretion in the centre.

Key words. Galaxies: interactions, irregular, starburst, individual: NGC 4418, VV 655

## 1. Introduction

The galaxy NGC 4418, at a distance of 34 Mpc, has a nucleus which is very bright in the infrared, but emits significantly less radio emission than expected from the FIR-radio correlation for star forming galaxies (Yun et al. 2001). Since Roche et al. (1986), multiple studies have presented observational evidence compatible with both a radio-weak AGN and/or a young starburst (see Sakamoto et al. (2013), Costagliola et al. (2013) and references therein).

Redshifted absorption lines have been found towards the galaxy's nucleus, for instance in the far-infrared OI and OH lines by González-Alfonso et al. (2012) with *Herschel*<sup>1</sup>, and in 21 cm by Costagliola et al. (2013) with the Multi-Element Radio Linked Interferometer Network (MERLIN) indicating infall of molecular and atomic gas. Sakamoto et al. (2013) also report a U-shaped feature visible in the optical extending towards the north-west, i.e. along the rotation axis of the disk, which they interpret as an outflow.

The NGC 4418 nucleus contains a Compton thick compact core (< 20 pc) surrounded by molecular gas (Sakamoto et al. 2013). The nucleus is deepely obscured, evidenced by the deep 9.7  $\mu$ m silicate absorption feature (Roche et al. 1986; Spoon et al. 2001) and the overall resemblance to an embedded protostar in the mid-IR (Spoon et al. 2001). If a starburst is powering the source, it is very deficient in PAH emission, likely caused by extreme conditions and extinction in the obscuring medium around the star forming regions. The H $\alpha$  emission from NGC 4418 is limited to the nucleus (Lehnert & Heckman 1995, their Fig 5, page 132), suggesting that the rest of the galaxy either lacks OB stars capable of exciting HII regions, or that HII gas in the disk is absent.

ALMA observations show a very rich spectrum of molecules in an environment similar to the nuclei of the extreme starburst galaxy Arp 220 (Costagliola et al. 2015). Costagliola et al. (2013) argue that if a central starburst is responsible for all the energy output, it must be 3-10 Myrs old and have a star formation rate >  $10\,M_\odot$  yr<sup>-1</sup>. The complex radio morphology reported by Varenius et al. (2014) indeed argues in favour of a significant starburst component. If this is the case, what triggered this recent starburst in the centre of NGC 4418?

<sup>&</sup>lt;sup>1</sup> Herschel is an ESA space observatory with science instruments provided by European-led Principal Investigator consortia and with important participation from NASA.

Roche et al. (1986) noted that NGC 4418 may be interacting with the nearby galaxy VV 655 (also known as MCG+00-32-013) about 3' South-East of NGC 4418. VV 655 has blue colors, irregular structure and emission lines consistent with vigorous star formation (Colless et al. 2003; Alam et al. 2015). Although this possible companion galaxy is shown by Kawara et al. (1990), their Fig. 1, and mentioned by Evans et al. (2003) and Costagliola et al. (2013), no clear evidence has been presented for any interaction between NGC 4418 and VV 655.

In this paper we present radio observations taken with the VLA to search for neutral hydrogen structures connecting NGC 4418 to VV 655. The paper is organised as follows. In Sect. 2 we describe the observations and data reduction. In Sect. 3 we present the results of analysis and modeling done using the data. The results are discussed in Sect. 4 and finally summarised in Sect. 5. In this paper we assume a distance to NGC 4418 (and VV 655) of  $34 \,\mathrm{Mpc}$ , i.e.  $1'' = 161 \,\mathrm{pc}$ , as given by Sakamoto et al. (2013).

## 2. Observations and data reduction

We present data from the VLA taken in D configuration in project AS748 (PI: H. Spoon) on 2003-03-21 with 5.3h on source. The parrallel hands (RR,LL) were correlated with phase-centre R.A.  $12^h26^m59^s.750$  and Dec.  $-00^\circ53'31.50''$  and the data stored in the archive with time resolution of 30 seconds and spectral resolution of 48.8 kHz per channel. The total bandwidth covered 63 channels, centered on 1.41017559 GHz.

The data were edited and calibrated in a standard manner using Astronomical Image Processing System (AIPS) (Greisen 2003) version 31DEC15. The Python-based interface to AIPS, ParselTongue (Kettenis et al. 2006), was used to script the calibration. The flux scale and bandpass was calibrated using 3C286, which was assumed to be 15.1025 Jy at the centre of the band as calculated by the AIPS task SETJY. The visibility phases were referenced to the calibrator 1150-003 at R.A.  $11^h50^m43.8707^s-00^\circ23'54.204''^2$ , found to be 2.94 Jy. The corrections derived from 3C286 and 1150-003 were applied to NGC4418. Visual inspection revealed HI-emission in the channel range 16-53. The remaining channels were used to fit and remove the continuum in the UV-domain using the task UVLSF in AIPS.

The continuum-subtracted data were imaged using the task CLEAN in CASA 4.6 with Briggs weighting (robust=1) using baselines >  $300\lambda$  (to filter out far-away interferring sources). During cleaning, the data were gridded in velocity (using the optical velocity definition), and CLEAN corrected for effects of the Earth's rotation and movement with respect to the solarsystem barycentre, assuming a HI rest-frequency of 1420.405751 MHz. A primary-beam corrected image cube was obtained of the stokes I emission with image pixel size 4''. The spectral cube had a velocity resolution of 10 km/s and RMS noise of  $\sim 0.4$  mJy beam $^{-1}$  in each velocity channel. A common synthesized CLEAN restoring beam of  $61.5'' \times 50.6''$  with position angle (PA)  $-1.19^\circ$  was used for all velocity channels.

We also obtained a 1.4 GHz continuum image by deconvolving the line-free output from UVLSF using the Multi-Frequency Synthesis gridding offered by CLEAN. The continuum image RMS noise was  $0.2\,\mathrm{mJy\,beam^{-1}}$  with a synthesized beam of  $61.5''\times51.0''$  with PA  $-1.34^\circ$ .

To get an independent estimate of the SFR we checked the  $70\,\mu m$  flux densities of NGC 4418 and VV 655 as observed by

Herschel PACS (Pilbratt et al. 2010; Poglitsch et al. 2010) using data from the Herschel Science Archive. We used data taken 2011-07-17 towards NGC 4418 with scan id 1342224340, available as a FITS image (with calibration level 2.5).

## 3. Results

In this section we present the results of the analysis of the continuum and spectral line images. Note that both images are available online via the CDS<sup>3</sup>.

#### 3.1. 1.4 GHz continuum

The 1.4 GHz continuum is presented in Fig. 1a as contours overlayed on a three colour (i,r,g-band) image made from the Sloan Digital Sky Survey (SDSS)  $^4$ . In addition to NGC 4418, four other sources are visible above  $4\sigma$  in Fig. 1a which are all identified as compact (<5'') sources with counterparts in the FIRST Survey (Becker et al. 1995) with the same flux density as measured in this work. Unfortunately we did not find any redshifts for these sources which could prove that they are background sources. However, given that they are compact, having no clear relation to either NGC 4418 or VV 655 (i.e. no extensions or alignments which could suggest e.g. AGN jet hot spots), and do not show any HI emission in Fig. 1b (i.e. indicate significantly different redshift) we assume these are background sources.

Assuming the eastern extension is a background source, a fit of a Gaussian intensity distribution to the image finds NGC 4418 to be unresolved with an integrated flux density of 40 mJy, in good agreement with the 38.5 mJy measured by Baan & Klöckner (2006) using the VLA. As noted by Costagliola et al. (2013), this is also in agreement with the 38 mJy measured with MER-LIN, which indicates that there is no significant 1.4 GHz emission on scales larger than the 0.5" component sampled by MER-LIN (Costagliola et al. (2013), their Fig. A.1).

## 3.1.1. Star formation rate estimates

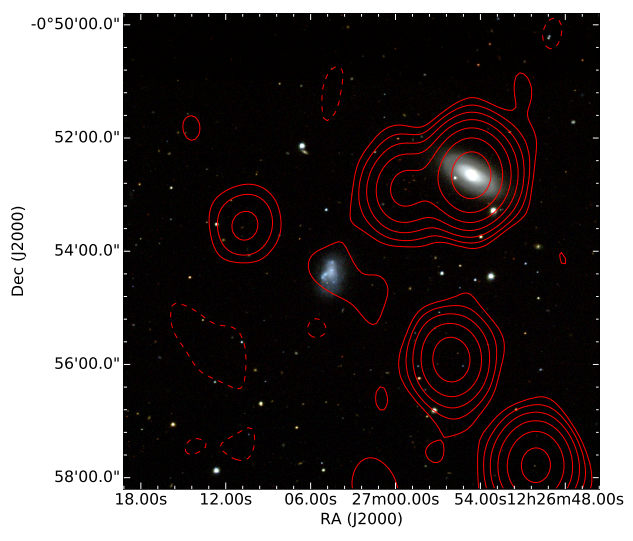
The galaxy VV 655 is barely detected at the  $3\sigma$  level in our  $1.4\,GHz$  continuum image (Fig. 1a) i.e.  $L_{1.4GHz}\sim8.2\times10^{19}\,W\,Hz^{-1}.$  Using Eq. 6 by Bell (2003) this corresponds to a star formation rate (SFR) of  $0.13\,M_{\odot}\,yr^{-1},$  although Bell (2003) states uncertainties as large as a factor of 5 for galaxies of this low luminosity. For comparison, using the same equation given the  $1.4\,GHz$  flux density of  $40\,mJy$  (5.53×10 $^{21}\,W\,Hz^{-1}$ ) we obtain an integrated radio SFR of  $3.2\,M_{\odot}\,yr^{-1}$  for NGC 4418.

From the Herschel 70 um image we measure 125 mJy associated with VV 655 which, assuming the same distance to VV 655 as for NGC 4418 of 34 Mpc, translates to  $L(70\mu\text{m}) = 7.39 \times 10^{41}\,\text{erg s}^{-1}$ . Calzetti et al. (2010) present a relation to estimate SFR from 70  $\mu\text{m}$  emission. While they do not claim accurate SFR estimates for individual galaxies, we use their Eq. 22 to get an order of magnitude estimate for VV 655 and we obtain SFR(70  $\mu\text{m}$ )~ 0.0435 M $_{\odot}\text{yr}^{-1}$ , i.e. within a factor of 3 from the 1.4 GHz estimate. We note, however, that VV 655 is below the validity limit of 1.4  $\times$  10<sup>42</sup> erg s $^{-1}$  stated by Calzetti et al. (2010) and therefore this value should be interpreted with caution. For comparion, using the same equation with the 39.3 Jy (2.33  $\times$  10<sup>44</sup> erg s $^{-1}$ ) measured at 70  $\mu$ m for NGC 4418 we estimate SFR(70  $\mu$ m)~ 13.7 M $_{\odot}$ yr $^{-1}$ . NGC 4418 is known to be ra-

<sup>&</sup>lt;sup>2</sup> Within 1 milliarcsecond of the current catalog position at http://astrogeo.org/calib/search.html.

<sup>&</sup>lt;sup>3</sup> See CDS URL

<sup>&</sup>lt;sup>4</sup> Using data from SDSS data release 12 (Alam et al. 2015) available via http://dr12.sdss3.org/mosaics/.



(a) 1.4 GHz continuum

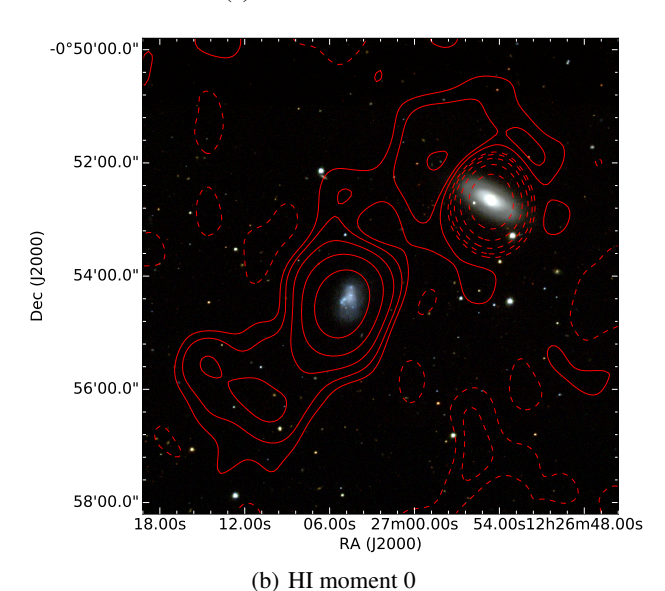


**Fig. 1.** Panel (a) shows the 1.4 GHz continuum plotted as contours of (–2, 2, 4, 8, 16, 32, 64, 128)×0.2 mJy beam<sup>-1</sup> overlayed on a three colour SDSS image (using i,r,g bands). NGC 4418 is the white disk in the topright part of the image, and VV 655 is the blue irregular galaxy near the image centre. In addition to NGC 4418, four other sources are visible above  $4\sigma$  as noted in Sect.3.1. VV 655 is barely detected at  $3\sigma$  in the radio continuum. Panel (b) shows the moment 0 map of the continuum-subtracted HI (in emission and absorption) with contours at  $(-32, -16, -8, -4, -2, 2, 4, 8, 16, 32) \times 35 \, \text{mJy beam}^{-1} \, \text{km s}^{-1}$ .

dio weak relative to the FIR-radio correlation (Yun et al. 2001) so SFR( $70 \mu m$ )>SFR(1.4 GHz) is expected.

#### 3.2. HI in emission and absorption

Fig. 1b shows the HI emission and absorption as a moment 0 map, produced by the task immoments in CASA. NGC 4418 is surrounded by HI seen in emission outside about 1' distance from the centre, and seen in absorption inside this radius (see Fig. 1b). HI emission is prominent towards VV 655 and in regions between the two galaxies. The moment 0 peak of absorption is -52 mJy beam<sup>-1</sup>km s<sup>-1</sup>, towards the centre of NGC 4418 and the peak of emission is 2.0 Jy beam<sup>-1</sup> km s<sup>-1</sup>, to-

wards centre of VV 655. A bridge of emission seem to connect VV 655 and NGC 4418, although this projection does not prove a physical connection - see further Sect. 3.2.2. Finally, there is prominent emission south-east of VV 655 with a peak of  $0.34\,\mathrm{Jy\,beam^{-1}km\,s^{-1}}$ .

The velocity structure of the gas is shown in projection as a moment 1 map in Fig. 2a, with moment 0 contours in black for easy comparison. The moment 1 map was obtained after first blanking pixels in the spectral cube with absolut value smaller than 1.6 mJy beam $^{-1}$ . This corresponds to selecting emission and absorption stronger than  $4\sigma$ , and was done to reduce influence from noise which is present also at velocities where there is no real emission or absorption. Although the spatial and spectral resolution is limited, a range of velocities are clearly detected from about  $2000\,\mathrm{km\,s^{-1}}$  to  $2250\,\mathrm{km\,s^{-1}}$ . This corresponds to emission both red- and blueshifted with respect to the velocity of  $2088\,\mathrm{km\,s^{-1}}$  measured for NGC 4418 by Sakamoto et al. (2013).

## 3.2.1. Position-velocity diagram and spectra

Fig. 2b shows a position-velocity (PV) diagram extracted from the spectral cube along the dashed line shown in Fig. 2a. Four distinct features can be seen at the approximate relative offset positions of -200'', -40'' (VV 655), 152" (NGC 4418; in absorption), and 212". Spectra extracted at these positions, i.e. the dashed lines in panel (b), are presented in Fig. 3.

The four spectra were modelled using two Gaussian intensity distributions each. The best fitted parameters are listed in Table 1. Although limited by spectral and spatial resolution, we note a tentative double structure in the first two panels (offsets -200" and -40"). We interpret the average HI velocity in the second panel towards VV 655, of  $2202 \pm 20 \,\mathrm{km}\,\mathrm{s}^{-1}$ , as the systemic velocity of the galaxy where the uncertainty on the central velocity is chosen to cover the two tentative peaks in the spectrum. The third panel, towards NGC 4418, is best fitted with two absorption components. While the component of Costagliola et al. (2013) fitted at  $2094 \pm 22 \,\mathrm{km} \,\mathrm{s}^{-1}$  is in excellent agreement with our result, their second HI component at  $2153 \pm 11 \,\mathrm{km \, s^{-1}}$  has significantly lower velocity than the one we find. This may be due to fitting constraints employed by Costagliola et al. (2013), who did not fit the two components simultaneously. The fourth panel corresponds to a region north-west of NGC 4418. In addition to redshifted absorption, we also see prominent blueshifted

Assuming the HI absorption from the 1.4 GHz continuum of 40 mJy dominates over HI emission towards NGC 4418, we can estimate the optical depth as  $\tau \approx -\ln(1+p/40 \text{mJy})$  where p are the (negative) peak values listed in Table 1. The estimated  $\tau$  for the two absorption components towards NGC 4418 are listed in Table 1.

## 3.2.2. An HI emission bridge between NGC 4418 and VV655

In Sect. 3.2.1 we noted the systemic HI velocities measured for VV 655 and NGC 4418 of  $2202 \pm 20 \, \mathrm{km \, s^{-1}}$  and  $2105.5 \pm 10 \, \mathrm{km \, s^{-1}}$  respectively. The spectral cube reveals HI-emission connecting VV 655 and NGC 4418. This structure is curved in three-dimensional (R.A., Dec., Velocity) space and cannot be well illustrated by a moment map (i.e. Figs. 1b and 2a) or a single PV diagram (such as Fig. 2b). To show this 3D-structure in two dimensions we plot three projections of the spectral cube in Fig. 4. In addition to the velocity axis, the velocity information

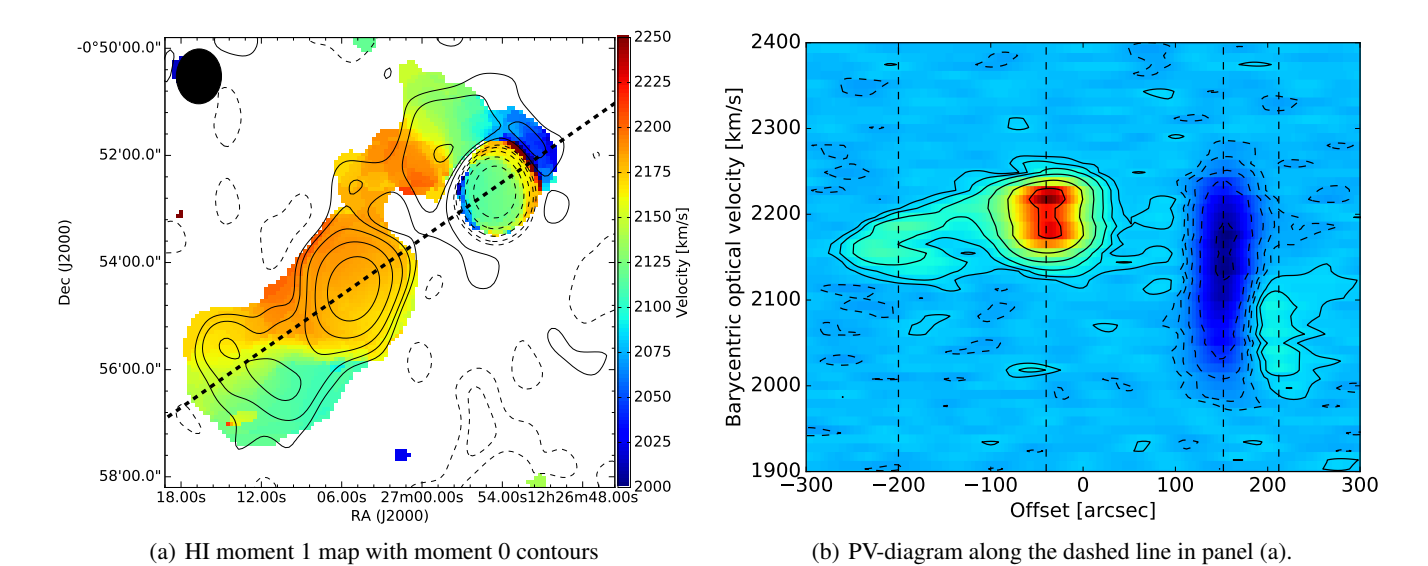
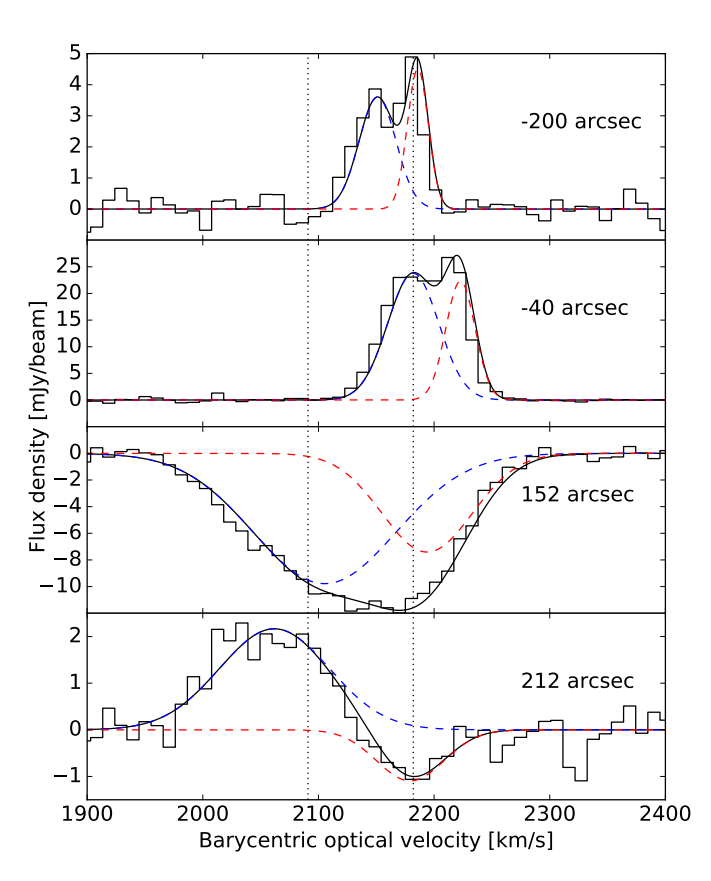


Fig. 2. Panel (a) shows the moment 1 HI map in color with the moment 0 contours from Fig. 1b in black. The CLEAN beam is displayed as a black ellipse in the top left corner. Panel (b) shows a Position-Velocity diagram extracted along the dashed line in panel (a); an 11.3' slice from R.A.  $12^h27^m21^s.547$  Dec.  $-00^\circ57'19.85''$  to R.A.  $12^h26^m44^s.380$  Dec.  $-00^\circ50'48.73''$ , i.e. going through both NGC 4418 and VV 655. Four distinct features can be seen along the slice at the approximate relative offset values of -200'', -40'' (VV 655), 152'' (NGC 4418; in absorption), and 212''. Spectra extracted at these positions, i.e. the dashed lines in panel (b), are presented in Fig. 3. Contours in panel (b) are  $\pm [0.025, 0.05, 0.1, 0.2, 0.4, 0.8] \times 26.7$  mJy/beam (the peak).



**Fig. 3.** Spectra extracted towards the four directions defined in Fig. 2b. The dashed curves show the fitted Gaussian components listed in Table 1. The solid line in each panel represents the sum of the fitted components, i.e. to be compared with the observed spectra in black steps. The vertical dotted lines show the velocities for the two components fitted to CO(2-1) by Costagliola et al. (2013). For reference, the systemic velocity of NGC 4418 has been measured as 2088 km/s by Sakamoto et al. (2013).

**Table 1.** Best fit parameters for the spectra shown in Fig. 3.

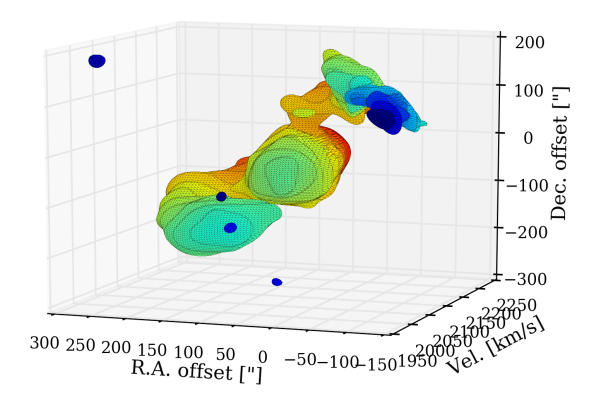
Offset	$v_c$	Peak	FWHM	$ au_p{}^a$
["]	[km/s]	[mJy/beam]	[km/s]	•
-200	2151.1±2.3	3.6±0.3	37.7±5.4	-
-200	2186.0±1.2	4.5±0.4	21.3±2.5	-
$-40^{b}$	2182.0±0.7	23.8±0.2	51.9±1.3	-
$-40^{b}$	2222.8±0.4	22.3±0.6	29.8±0.8	-
$152^{c}$	2105.4±10.0	-9.8±0.6	145.1±12.8	0.28
$152^{c}$	2194.0±4.4	-7.4±1.6	92.2±8.3	0.21
212	2061.9±5.1	2.2±0.2	112.0±13.0	-
212	2179.4±7.7	$-1.1\pm0.2$	68.7±17.5	-

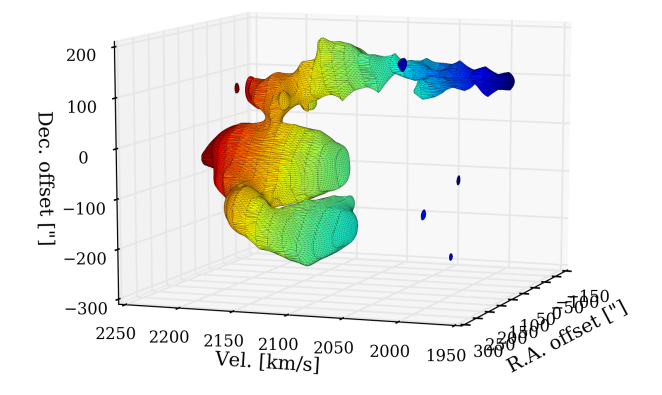
**Notes.** <sup>(a)</sup> Assuming an unresolved background continuum of 40 mJy from NGC 4418 as noted in Sect. 3.1. <sup>(b)</sup> Towards VV 655. <sup>(c)</sup> Towards NGC 4418.

is also reflected in the color map. Note that the projections only show emission (not absorption), and only pixels brighter than  $4\sigma$  i.e.  $1.6\,\mathrm{mJy/beam}$  to reduce influence of noise. An animated GIF-image showing more projections are available in the online material accompanying this paper. From the three-dimensional data it is clear that there is an HI emission bridge connecting NGC 4418 and VV 655.

# 3.3. Correction for HI absorption

As noted in Sect. 3.1, the 1.4 GHz continuum from NGC 4418 appears unresolved in these observations. However, the limited angular resolution of our data causes absorption towards the nucleus to blend outwards, reducing nearby emission. To obtain better estimates of the true HI emission, we therefore corrected for the unresolved absorption in the cube. This was done by assuming the absorption to be unresolved in each velocity channel, and therefore completely described by the value of the minimum pixel in each channel. To account for noise variations and pixel size limitations we allowed the minimum position to vary between the channels. The variations were limited to the minor





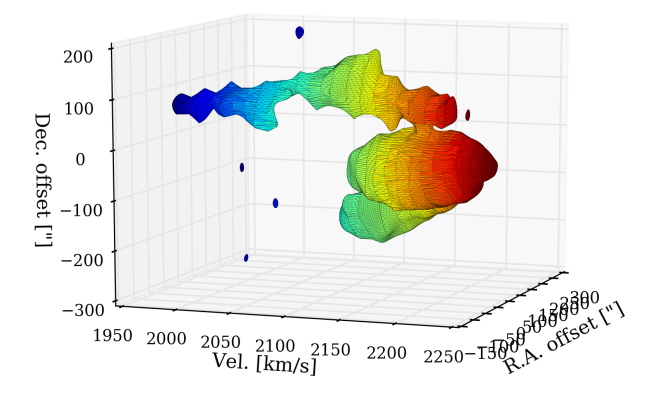


**Fig. 4.** Three projections of the continuum-subtracted HI data cube (R.A., Dec., velocity) showing the arc-like connection between NGC 4418 and VV 655 in HI emission. For reference, the systemic HI velocities for VV 655 and NGC 4418 are  $2202 \pm 20 \,\mathrm{km \, s^{-1}}$  and  $2105.5 \pm 10 \,\mathrm{km \, s^{-1}}$  respectively (see Sect. 3.2.1). Note that this figure only shows the emission, not the absorption towards NGC 4418.

beam FWHM of 12 pixels around the NGC 4418 position, but the actual shift of the minimum position was less than 3 pixels between all channels.

In each velocity channel with negative values towards NGC 4418, we subtracted the CLEAN beam multiplied with the minimum pixel value, i.e. assuming an unresolved background continuum. The strong absorption feature towards NGC 4418 was successfully removed (supporting our single-pixel assumption) and we now recover more HI emission close to NGC 4418,

**Table 2.** Integrated HI emission flux measurements for the three regions defined in Fig. 5 together with corresponding HI mass estimates from Eq. 1. Note that these values were obtained after removing the absorption towards NGC 4418 as described in Sect. 3.3.

Region	Flux [Jy km s <sup>-1</sup> ]	$M_{\rm HI}~[{ m M}_{\odot}]$
North (NGC 4418)	1.47	$4.0 \cdot 10^{8}$
Middle (VV 655)	4.05	$11.0 \cdot 10^8$
South	0.83	$2.3 \cdot 10^8$
Sum	6.35	$17.3 \cdot 10^8$

see Fig. 5 and compare with Fig. 1b. While we restricted our subtraction to pixels with negative values, there may still be absorption present which reduce the emission in some channels, although not below zero, i.e the emission is not optically thin. Furthermore, we note that our method of correcting for the absorption cannot recover any HI emission from the nucleus of NGC4418. These effects may explain the remaining weak depression in the emission towards NGC 4418 in Fig. 5.

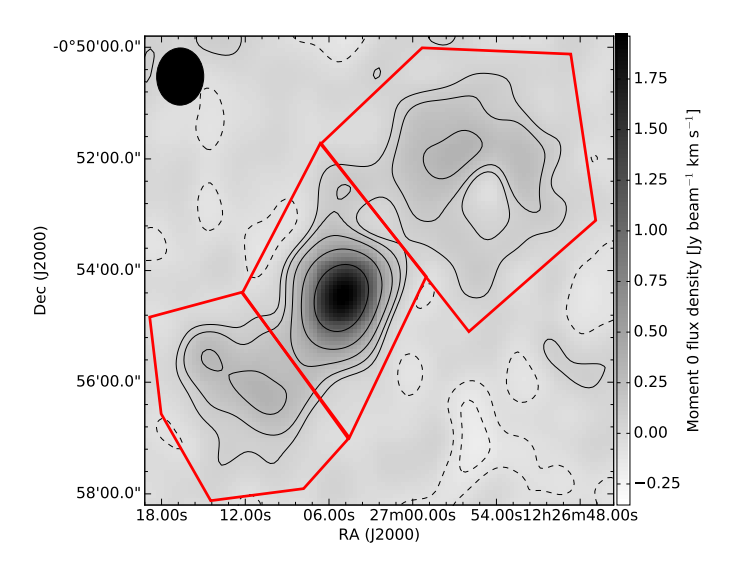


**Fig. 5.** Moment 0 map of HI after correcting for the absorption towards NGC 4418 as described in Sect. 3.3. More emission is seen close to NGC 4418 than in Fig. 1b. The red polygons mark three regions where pixels were summed to measure the flux values listed in Table. 2. Both grayscale and contours show the moment 0 map, with the same contours as in Fig. 1b.

### 3.3.1. HI emission fluxes and mass estimates

To measure the integrated flux density of the HI emission we have divided the emission in three regions in Fig. 5: *North*, defined as the top-right polygon, includes emission associated with NGC 4418. The *Middle* polygon includes emission associated with VV 655, and the *South* polygon includes emission associated with the south-east extension from VV 655. The correction for absorption towards NGC 4418 makes it possible to estimate the HI gas mass from emission associted also with NGC 4418. This value is a lower limit since the emission may not be optically thin as noted in Sect. 3.3. The HI emission flux for the three regions was measured by summing pixels in a moment 0 map, and are given in Table 2.

From the detected HI emission we estimate the HI mass using Eq. 13.57 in Wilson et al. (2009):

$$M_{\rm HI}[{\rm M}_{\odot}] = 2.36 \times 10^5 D^2 \int S_{\nu} d\nu$$
 (1)

where  $\int S_{\nu} d\nu$  is integrated line flux in Jy km/s, and *D* is the distance in Mpc. With D=34 Mpc we obtain the values listed in Table 2. We note that the estimated HI mass of VV 655 is very similar to the HI masses of other blue compact dwarf galaxies measured by Thuan et al. (2016).

## 4. Discussion

In this section we discuss the results presented in the previous section.

### 4.1. NGC 4418 and VV 655 are interacting

The spectral cube presented in Sect. 3.2.2 shows that NGC 4418 and VV 655 are connected by a bridge of atomic hydrogen seen in emission. Furthermore, the similar velocities of the gas surrounding VV 655 and NGC 4418 and the elongated gas morphology can all be explain as signatures of a recent or ongoing interaction process, where the elongated HI structure connecting the two galaxies may have formed when the more massive NGC 4418 disturbed the HI surrounding VV 655. We propose that at some time, relatively recently, NGC 4418 was gas poor while VV 655 had a significant HI envelope. As the galaxies passed each other, the more massive NGC 4418 stripped away HI gas from VV 655. This interaction formed the elongated HI structure we see today. Indeed, the HI morphology is similar to the structure seen in other interacting pairs in the HI Rogues Gallery (Hibbard et al. 2001). For example, the interacting pair Galaxy Pair II ZW 70/71 (UGC 9562 and UGC 9560) have an HI emission bridge connecting the two galaxies and an HI extension from one of the galaxies (Cox et al. 2001).

As the HI gas is *only* elongated, and thus the structure is relatively simple, it is possible that these two galaxies are only passing once. This could explain the young age of the star burst in the centre of NGC 4418, as the swept up gas need time to cool enough to reach the centre of the galaxy. The tidal forces caused by the interaction can also explain the HI emission extending south-east of VV 655. From the data it is however not clear if the galaxies are now bound in a merging system or if they are just passing each other once. Detailed modeling of the velocity structure would require data with higher spatial and spectral resolution and is beyond the scope of this paper.

# 4.2. HI falling towards NGC 4418

The redshifted absorption detected towards NGC 4418 (see panel 3 in Fig. 3) implies gas in front of NGC 4418 travelling towards the galaxy. Indeed, the velocity of about 90 km/s relative to NGC 4418 is similar to the redshifted CO(2-1) component found by Costagliola et al. (2013). This is consistent with infall, but because of the limited spatial resolution we cannot probe the detailed dynamics around NGC4418. While a significant amount of HI gas is falling towards NGC4418, it is not clear from these data if this gas does fall all the way into the centre of the galaxy. However, if some of the gas does reach the centre, it can explain the recent star formation and/or AGN activity in the galaxy nucleus.

#### 4.3. The north-west outflow

North-west of NGC 4418 we detect HI in emission blueshifted with respect to the systemic velocity of the galaxy. The blueshift can be explained if the gas is being pushed with an inclination towards us, i.e. out from the galaxy nucleus. Indeed, the orientation of this emission is consistent with being a large-scale continuation of the outflow signature seen by Sakamoto et al. (2013), their Fig. 16. It is possible that the activity in the nucleus is powering and outflow which pushes out HI gas surrounding the galaxy. This argument is supported by the fact that there is no other source visible in this region which could be the source of this emission. Such an outflow can be driven by either intense star formation or AGN activitiy, or a combination of both.

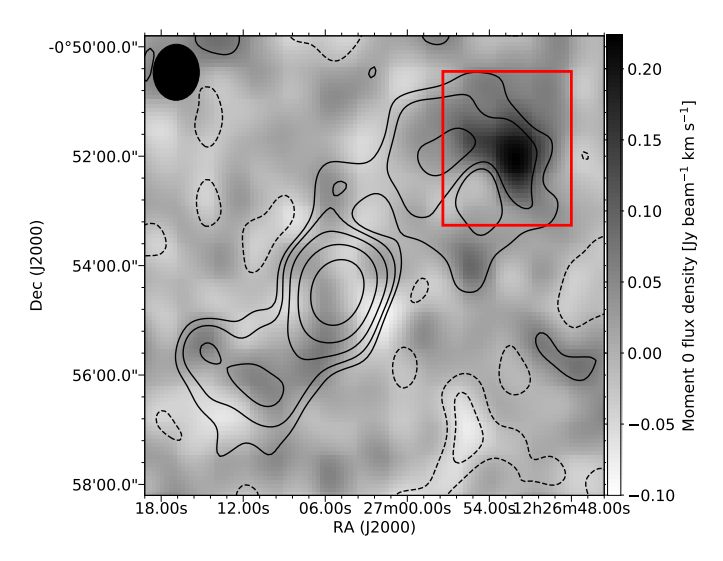


**Fig. 6.** In grayscale: moment 0 map of 19 most blueshifted channels, after first removing the absorption towards NGC 4418 as described in Sect. 3.3. Contours are the same as in Fig. 5 to guide the eye. The red polygon mark regions where pixels were summed to measure the flux of the outflow, discussed in Sect. 4.3

To measure the HI emission associated with the outflow, we used the absorption-subtracted image cube (see Sect. 3.3) to produce a moment 0 map, including only the channels containing blueshifted emission associated with the outflow position. This moment 0 map is shown in grayscale in Fig. 6. Summing the pixels in the marked region in Fig. 6 we measure a flux of 0.48 Jy beam $^{-1}$  km s $^{-1}$  associated with the outflow, which using Eq. 1 translates to an atomic hydrogen gas mass of  $1.3\times10^8~M_{\odot}$ .

We note that the outflow is not clearly resolved in most velocity channels. As an approximation of the outflow volume, we assume a cylinder with diameter 25" (equal to half the minor axis of the CLEAN restoring PSF) and length 60" (equal to the distance from the centre of NGC 4418 to the peak of the outflow emission in Fig. 6. Given the HI mass estimate above, this implies an average outflow density of  $1.1 \times 10^6 \, M_\odot \, \mathrm{kpc}^{-3}$ . This is an upper limit, given that the outflow structure is likely conical instead of a cylinder, as evident from Sakamoto et al. 2013, their Fig. 16.

To estimate the mass outflow rate we need the de-projected outflow velocity. As an upper limit we take the velocity of the most blueshifted velocity channel with emission brighter than  $3\sigma$ , which gives a velocity of 2004 km s-1. (This velocity can also be approximately determined from Fig. 2b or the lowest panel in Fig. 3, but using the full cube provides maximum precision.) Taking the systemic velocity for NGC 4418 of 2088 km s<sup>-1</sup>

from Sakamoto et al. (2013) implies an outflow speed of 84 km/s. Assuming the outflow is perpendicular to the galaxy disk, which has an inclination angle of  $62^{\circ}$  (Sakamoto et al. 2013), we obtain a de-projected outflow velocity of  $178 \, \mathrm{km \, s^{-1}}$ . We note that this is similar to the projected minor-axis velocity shear of  $200 \, \mathrm{km \, s^{-1}}$  measured in [N<sub>II</sub>] as noted by Sakamoto et al. (2013).

Given the above assumptions, we estimate a mass outflow rate of  $2.5\,M_\odot\,yr^{-1}$ . This estimate is to be taken as an order of magnitude estimate. More accurate constraints require observations with higher spatial resolution and sensitivity, to properly study the HI velocity structure on scales between those sampled by MERLIN as presented by Costagliola et al. (2013) and those sampled by VLA as presented in this work.

# 5. Summary

We present observations at 1.4 GHz with the VLA of radio continuum, as well as emission and absorption from atomic hydrogen, towards the galaxies NGC 4418 and VV 655. We detect a large (5′  $\sim 50\, kpc$ ) HI structure in emission, connecting the two galaxies. While NGC 4418 is bright in continuum emission and seen in HI absorption, VV 655 is barely detected in the continuum but show bright HI emission ( $M_{HI} \sim 10^9\, M_{\odot}$ ). We estimate SFRs from the 1.4 GHz continuum of 3.2  $M_{\odot}\, yr^{-1}$  and 0.13  $M_{\odot}\, yr^{-1}$  for NGC 4418 and VV 655 respectively.

We fit Gaussian intensity distributions to spectra extracted from the image cube and measure systemic HI velocities of  $2202 \pm 20\,\mathrm{km\,s^{-1}}$  (emission) and  $2105.4 \pm 10\,\mathrm{km\,s^{-1}}$  (absorption) for VV 655 and NGC 4418 respectively. We also detect redshifted HI absorption ( $v_c = 2194.0 \pm 4.4\,\mathrm{km\,s^{-1}}$ ) towards NGC 4418 which suggests gas infall. The morphology and velocity structure seen in HI is consistent with an interaction scenario, where gas was transferred from VV 655 to NGC 4418. Some gas is falling towards NGC 4418, and may fuel the activity in the centre.

North-west of NGC 4418 we detect HI in emission, blueshifted with respect to NGC 4418, consistent with an outflow perpendicular to the galaxy disk. We interpret blueshifted HI-emission north-west of NGC 4418 as a continuation of the outflow previously discussed by Sakamoto et al. (2013), powered by star formation and/or black hole accretion in the centre. The observed maximum velocity of  $v_c = 2004 \, \mathrm{km \, s^{-1}}$  imples a deprojected speed of 187 km s<sup>-1</sup>. Assuming a steady-state cylindrical outflow from the core of NGC 4418, we obtain an order of magnitude estimate of the HI mass outflow rate as 2.5 M<sub> $\odot$ </sub> yr<sup>-1</sup>.

Acknowledgements. F.C. acknowledges support from Swedish National Research Council grant 637-2013-7261. This research made use of APLpy, an open-source plotting package for Python (Robitaille & Bressert 2012). Using data from the Karl G. Jansky Very Large Array (VLA), we acknowledge that the National Radio Astronomy Observatory is a facility of the National Science Foundation operated under cooperative agreement by Associated Universities, Inc. Funding for SDSS-III has been provided by the Alfred P. Sloan Foundation, the Participating Institutions, the National Science Foundation, and the U.S. Department of Energy Office of Science. The SDSS-III web site is http://www.sdss3.org/. The authors acknowledge assistance from Joachim Wiegert and Niklas Falstad with obtaining Herschel  $70\,\mu\mathrm{m}$  SFR estimates. The authors also want to thank John Hibbard for discussions during the preparation of this manuscript. Finally, the authors acknowledge the constructive feedback offered by the anonymous referee which helped to improve the quality of this paper.

#### References

Alam, S., Albareti, F. D., Allende Prieto, C., et al. 2015, ApJS, 219, 12 Baan, W. A. & Klöckner, H.-R. 2006, A&A, 449, 559 Becker, R. H., White, R. L., & Helfand, D. J. 1995, ApJ, 450, 559

Bell, E. F. 2003, ApJ, 586, 794

Calzetti, D., Wu, S.-Y., Hong, S., et al. 2010, ApJ, 714, 1256

Colless, M., Peterson, B. A., Jackson, C., et al. 2003, ArXiv Astrophysics eprints

Costagliola, F., Aalto, S., Sakamoto, K., et al. 2013, A&A, 556, A66 Costagliola, F., Sakamoto, K., Muller, S., et al. 2015, A&A, 582, A91

Cox, A. L., Sparke, L. S., Watson, A. M., & van Moorsel, G. 2001, AJ, 121, 692 Evans, A. S., Becklin, E. E., Scoville, N. Z., et al. 2003, AJ, 125, 2341

González-Alfonso, E., Fischer, J., Graciá-Carpio, J., et al. 2012, A&A, 541, A4 Greisen, E. W. 2003, Information Handling in Astronomy - Historical Vistas, 285, 109

Hibbard, J. E., van Gorkom, J. H., Rupen, M. P., & Schiminovich, D. 2001, in Astronomical Society of the Pacific Conference Series, Vol. 240, Gas and Galaxy Evolution, ed. J. E. Hibbard, M. Rupen, & J. H. van Gorkom

Kawara, K., Taniguchi, Y., Nakai, N., & Sofue, Y. 1990, ApJ, 365, L1

Kettenis, M., van Langevelde, H. J., Reynolds, C., & Cotton, B. 2006, in Astronomical Society of the Pacific Conference Series, Vol. 351, Astronomical Data Analysis Software and Systems XV, ed. C. Gabriel, C. Arviset, D. Ponz, & S. Enrique, 497

Lehnert, M. D. & Heckman, T. M. 1995, ApJS, 97, 89

Pilbratt, G. L., Riedinger, J. R., Passvogel, T., et al. 2010, A&A, 518, L1

Poglitsch, A., Waelkens, C., Geis, N., et al. 2010, A&A, 518, L2

Robitaille, T. & Bressert, E. 2012, APLpy: Astronomical Plotting Library in Python, Astrophysics Source Code Library

Roche, P. F., Aitken, D. K., Smith, C. H., & James, S. D. 1986, MNRAS, 218, 19P

Sakamoto, K., Aalto, S., Costagliola, F., et al. 2013, APJ, 764, 42

Spoon, H. W. W., Keane, J. V., Tielens, A. G. G. M., Lutz, D., & Moorwood, A. F. M. 2001, A&A, 365, L353

Thuan, T. X., Goehring, K. M., Hibbard, J. E., Izotov, Y. I., & Hunt, L. K. 2016, MNRAS

Varenius, E., Conway, J. E., Martí-Vidal, I., et al. 2014, A&A, 566, A15Wilson, T. L., Rohlfs, K., & Hüttemeister, S. 2009, Tools of Radio Astronomy (Springer-Verlag)

Yun, M. S., Reddy, N. A., & Condon, J. J. 2001, ApJ, 554, 803